Polymer Testing 83 (2020) 106321

Contents lists available at ScienceDirect

Polymer Testing

journal homepage: http://www.elsevier.com/locate/polytest

Replication and surface properties of micro injection molded PLA/MWCNT nanocomposites

Joo Hyung Lee [a,1], Sang Ho Park [b,1], Seong Hun Kim [a,*], Hiroshi Ito [c]

[a] Department of Organic and Nano Engineering, College of Engineering, Hanyang University, Seoul 04763, South Korea
[b] LG Hausys, R&D Center, Seoul, South Korea
[c] Department of Polymer Science and Engineering, College of Engineering, Yamagata University, 4-3-16 Jonan, Yonezawa, Yamagata, 992-8510, Japan

ARTICLE INFO

Keywords:
Polylactide
Micro injection molding
Carbon nanotube
Replication property

ABSTRACT

Multi-walled carbon nanotube (MWCNT) reinforced polylactide (PLA) nanocomposites were injected molded into a mold with micro needle patterns. In order to alleviate the hesitation effect caused by an increased melt viscositgy of PLA/CNT nanocomposites, the effects of the injection speed and holding pressure on the replication property were investigated. The effects of MWCNTs on the crystallization, thermal behavior, replication properties, replication and surface properties of micro injection molded PLA/CNT nanocomposites were investigated. An analysis of crystallinity and thermal behavior indicated that the MWCNTs promoted the unique α' to α crystal transition of PLA, leading to an enhancement of surface modulus and hardness, as measured using a nano-indentation technique. The specific interaction between PLA and MWCNTs was characterized using an equilibrium melting point depression technique. Furthermore, the MWCNTs increased the activation energy for thermal degradation of PLA due to the physical barrier effect. The improved replication quality of the microfeatures in the PLA/MWCNT nanocomposites has been achieved by elevating injection speed and holding pressure, which enhances the polymer filling ability within the micro cavity. A replication ratio greater than 96% for the micro injection molded PLA/CNT nanocomposites were achieved at holding pressure of 100 MPa and injection speed of 120 mm/s. This study shows that processing conditions significantly influence the replication and surface properties of micro injection molded PLA/CNT nanocomposites.

1. Introduction

Micro injection molding is core technology for the fabrication of micro polymeric products such as micro gear, fluidic devices, electro-mechanical systems, and medical devices because of its cost-effectiveness and capability for mass production [1–4]. The effects of the internal structure of the injection mold products [5,6], process parameters [7], and geometric factors [8–11] have been extensively investigated. In applications of micro injection molding, the replication quality of microfeatures is an important factor that determines the reliability of the selected processing route [12]. On the other hand, if polymer melt filling a cavity has the option of filling either a thick section or a thin section, the polymer tend to fill the thick section first. This results in the flow of polymer in the thin route stopping or slowing significantly, namely "hesitation effect" (Scheme 1). Since the hesitation can reduce part quality due to poor packing, high stresses, and non-uniform orientation, an optimization of process conditions is required. The flow of polymer melts, which determine surface quality in micro cavities is affected by various factors, including process parameters, material rheology, and machine design. With regard to process optimization, the mold temperature [13], holding pressure, and injection speed [12] are regarded as the major factors, determining the surface quality of microfeatures. However, an increase in the mold temperature is not appropriate for improving surface quality because it increases the cycling time of the process, thus increasing production costs. Therefore, the effects of increasing the holding pressure and injection speed on the surface quality were evaluated in this research.

Among the various polymer materials suitable for micro injection molding, renewable resources derived polylactide (PLA) has been intensively investigated [14] and is expected to replace petroleum-based polymers because of its biodegradability [15–17], biocompatibility [18,19], and lack of toxicity to the human body, which facilitates biomedical

* Corresponding author.
E-mail address: kimsh@hanyang.ac.kr (S.H. Kim).
[1] Both authors contributed equally to this work.

https://doi.org/10.1016/j.polymertesting.2019.106321
Received 30 August 2019; Received in revised form 16 December 2019; Accepted 29 December 2019
Available online 10 January 2020

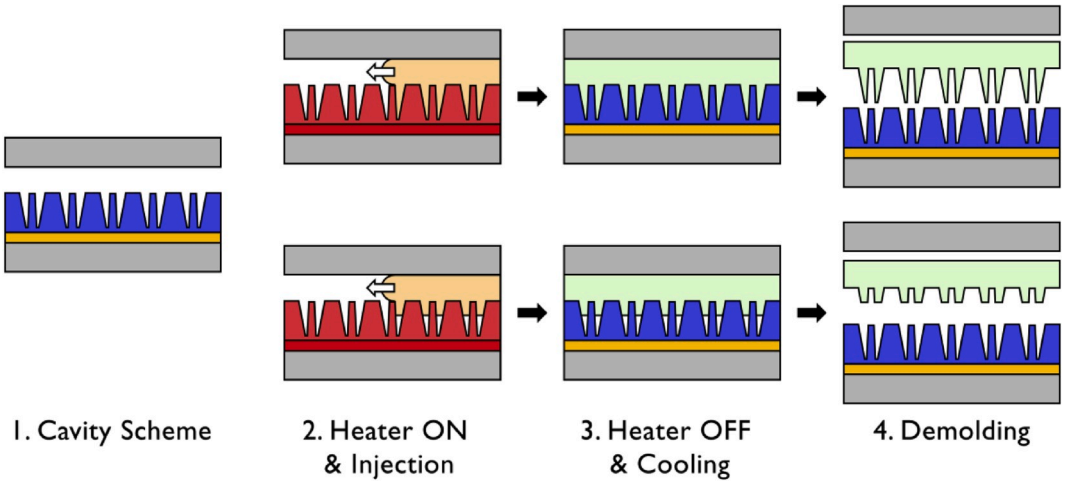

Scheme 1. Scheme of a typical micro-injection molding process (upper) and a hesitation effect of the melt flow in micro needle patterns (lower).

and pharmaceutical applications [20,21]. Nevertheless, the widespread application of pure PLA is limited because of its extremely slow crystallization rate, which prolongs the processing cycle, resulting in increased production costs [22].

As PLA is a semi-crystalline polymer [23,24], its mechanical and physical properties are governed by controlling the crystallization process. Nanoscale reinforcement in order to enhance the polymer properties is expected to change the crystallization behavior of PLA [25–27]. Therefore, research to promote the crystallization of PLA by incorporating various nucleating agents such as talc [28], clay [29–32], starch [33], and cellulose nanocrystals [34], has been conducted.

Among various nanofillers, carbon nanotubes (CNTs) are effective in enhancing the physical properties and crystallization of PLA [35–37] because of their own excellent physical properties, including their high aspect ratio and large surface area [38]. Our previous research [39] has indicated that CNTs have a significant nucleation effect on PLA even at a very low loading level of 0.2 wt%, at which the half crystallization time of isothermal crystallization is remarkably decreased, from 22.1 to 5.9 min, at 120$_o$C. PLA can be crystallized in α-, β-, and γ-phases, depending on the conditions [40–42]. The α-phase, the most common and stable polymorph, with a left-handed 10/3 helix, can be obtained from a melt or solution under normal conditions [40]. The β-phase, with a left-handed 3/1 helix, can be obtained by stretching the α-phase at higher draw ratios and drawing temperatures [41,43]. The γ–phase can be obtained by epitaxial growth on the hexamethylbenzene substrate [42,43]. A new crystal form, named the α′-form, is a disordered crystal form and presents in PLA crystallized at lower temperatures [44]. Pan et al. [43] reported that the transition of PLA crystals from the disordered crystal (α′-phase) to the ordered crystal (α-phase) occurred during the annealing process and depended on the annealing time and temperature. This transition is more prominent in the presence of CNTs [45]. Numerous studies on nanoindentation of injection molded polymers suggest that for the crystallinity affects both modulus and hardness [46,47]. Furthermore, the molded polymers may experience uneven cooling rates between outer and inner part. Therefore, the increased crystallization rate promoted by incorporation of CNT may affect surface properties. However, the addition of CNT into PLA leads to an increase in the complex viscosity, storage modulus, and loss modulus, which is more pronounced in the low frequency range than the high frequency range. This indicates that the PLA/CNT nanocomposites are more elastic that neat PLA, which can lead to the hesitation effect mentioned above in micro injection molding process.

In this study, to overcome the drawbacks in replication of high loaded PLA/CNT nanocomposites, optimal conditions for micro injection molding were studied. After the annealing process, the surface modulus and hardness of PLA were found to be improved by the addition of CNTs, which leads to an α-phase transition in the PLA/CNT nanocomposites, and this transition was confirmed by thermal and crystallinity analyses. The interaction between CNT and PLA, and thermal stability were also investigated.

Table 1
Experimental conditions for micro injection molding process.

	Process condition
Injection temperature (°C)	210
Injection pressure (MPa)	200
Mold temperature (°C)	55
Cooling time (s)	10
Velocity-pressure position (s)	3
Injection speed (V, mm/s)	30, 60, 90, 120
Holding pressure (P, MPa)	60, 80, 100

2. Experimental

2.1. Materials and preparation of nanocomposites

Commercial PLA (4032D, M_n = 52,000 g/mol) in pellet form was purchased from Cargill-Dow Inc. and MWCNTs (purity >95%) synthesized by thermal chemical vapor deposition were obtained from Iljin Nanotech, Korea. The diameter and length of MWCNTs were 10–40 nm and 10–50 μm, respectively, yielding an aspect ratio of about 1000. The melt compounding of PLA with 0.02, 0.05, 0.1, and 0.2 wt% MWCNTs was conducted using a HAAKE rheometer (HAAKE Technik GmbH, Germany) equipped with a twin-screw extruder. The temperature of the heating zone was maintained at 185, 190, 195, and 185 °C from hopper to die with a constant screw speed of 20 rpm.

2.2. Micro injection molding

A small electric injection molding machine (ELJECT AU3E; Nissei Plastic Industrial Co., Ltd.) was used for micro injection molding. The processing conditions for micro injection molding are listed in Table 1. To investigate the effect of the injection molding conditions on surface replication quality, PLA/MWCNT nanocomposites were injection molded at different injection speeds (V) and holding pressures (P). The geometry of the mold with micro needle patterns is described in Fig. 1(a). A mold with micro needle patterns of 5x5 pieces inside the 10x10x1 mm^3 cavity was used. The hole and needle diameters were 100 and 26 μm, respectively. The hole depth was 50 μm.

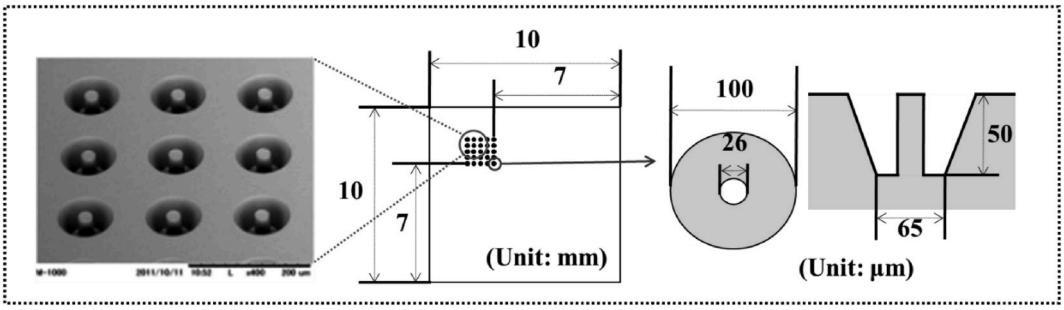

Fig. 1. Geometry of the mold with micro needle patterns.

2.3. Characterization

2.3.1. Crystallinity

Wide-angle X-ray diffraction (XRD) analysis was conducted using a D/MAX-2500 X-ray generator (Rigaku Denki) with Ni-filtered CuKα X-rays (λ = 0.1542 nm) over the 2θ range of 5–45° at a scan speed of 2°/min.

2.3.2. Thermal properties

The thermal behaviors of the PLA/MWCNT nanocomposites were investigated through differential scanning calorimetry (DSC), DSC7 (PerkinElmer), over a temperature range of 30–200 °C at a heating rate of 10 °C/min under an atmosphere of nitrogen. To conduct Hoffman-Weeks plots, isothermal crystallizations of PLA/MWCNT nanocomposites were performed by DSC. The samples were heated to 200 °C at a heating rate of 10 °C/min and maintained at 200 °C for 10 min to remove any previous thermal history, and then quenched at −170 °C/min to the desired crystallization temperature within a range of 90–130 °C, and held for 60 min for complete isothermal crystallization. The second heating was performed at a rate of 10 °C/min. To obtain the equilibrium melting temperature (T^0_m), the melting temperatures (T_m) measured from the endothermic peaks were plotted versus the crystallization temperatures (T_c), and the T^0_m values were obtained from the extrapolated intersections of the T_m vs T_c lines for various MWCNT contents with the $T_m = T_c$ line. For investigation of thermal stability, thermogravimetric analysis (TGA) of the PLA/MWCNT nanocomposites was performed with a PerkinElmer Pyris 1 thermogravimetric analyzer over a temperature range of 30–600 °C at a heating rate of 15 °C/min in nitrogen.

2.3.3. Replication quality

The replication ratio was calculated as the ratio of the height of surface structure to the depth of the mold, as measured using laser spectroscopy (LEXT OLS 4000, Olympus, Japan) [4]. The morphology of microstructures in the micro injection molded nanocomposites was observed using a JEOL JSM-6340F scanning electron microscope (SEM). The melt flow rate (MFR) was measured to investigate the melt flow of PLA/MWCNT nanocomposites in the mold using a Melt Indexer F–F01 (Toyoseiki, Japan). The MFR was obtained by measuring the amount of the extrudate for 10 min under a load of total mass of 2.16 kg at a temperature of 190 °C.

2.3.4. Nanoindentation

The nanoindentation measurements were performed using an MTS Nano Indenter XP (MES; Nano Instruments Innovation Center, TN, USA) with a continuous stiffness measurement technique [48]. The method of nanoindentation, including this technique, has been well described by Fischer-Cripps [49]. A three-sided pyramid (Berkovich) diamond indenter was used for the indentation tests. The best-replicated samples were utilized and annealed at 120 °C for 5 min for nanoindentation measurements. Before the experiments, micro injection molded PLA/MWCNT nanocomposites were mounted on flat aluminum stubs using superglue. The indenter was pressed into the smooth surface of the samples at a constant strain level to avoid any strain-hardening effect in the indentation experiments [50].

3. Results and discussion

3.1. Crystallinity

XRD patterns of PLA/MWCNT nanocomposites after an annealing process at 120 °C for 5 min and 60 min are shown in Fig. 2 (a) and (b). After the 5 min annealing process, the neat PLA exhibited weak diffraction peaks at 2θ = 16.4° and 18.7°, corresponding to (200)/(110) and (203) reflections of the α'-phase of PLA [44], respectively; this form has looser chain packing and disordered packing of the side groups in the helical chains [51–53]. The disordered α'-phase of PLA is found to form when the crystallization temperature (T_c) is below 100 °C, while the ordered α-phase of PLA is found to form preferentially at a T_c above 120 °C, implying that the two crystal forms of PLA coexist between 100 and 120 °C [54]. As shown in Fig. 2(a), the intensity of the peak corresponding to (200)/(110) increased with the MWCNT content, indicating a fast packing rate because of the strong nucleating ability of MWCNTs during the 5 min annealing process. The diffraction peaks

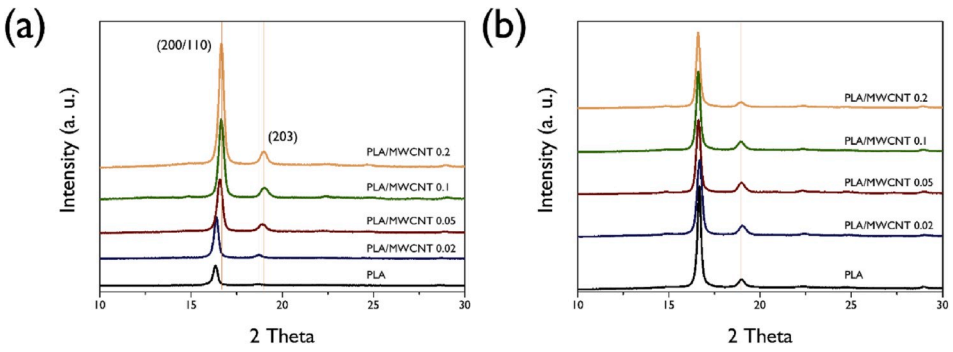

Fig. 2. XRD patterns of the neat PLA and PLA/MWCNT nanocomposites after crystallization at 120 °C for 5 min (a) and 60 min (b).

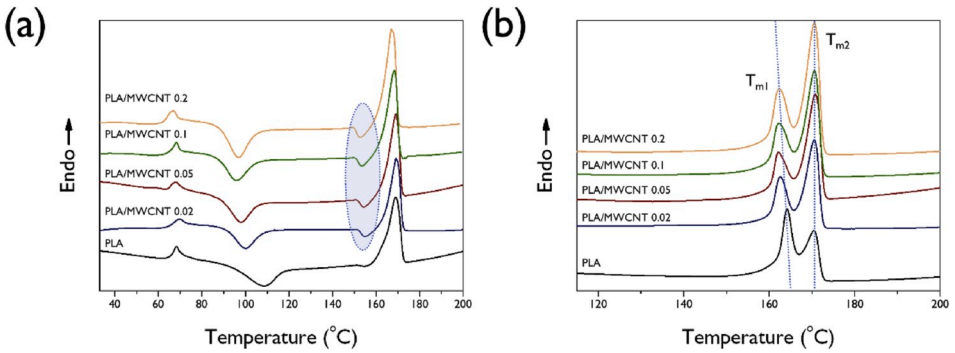

Fig. 3. DSC thermograms of the neat PLA and PLA/MWCNT nanocomposites before (a) and after crystallization process at 120 °C (b).

around 16.7° and 19.1° are assigned to the ordered α-phase of PLA [55] and the two distinct diffraction peaks at 16.4° and 18.7° were shifted to 16.6° and 18.9°. These results indicated that the MWCNTs assisted the disorder-to-order (α'-to-α) transition of PLA and led to more compact chain packing of the crystal lattice during the 5 min annealing process. However, after the 60 min annealing process, the intensity of the peak corresponding to the ordered α-phase decreased with the addition of MWCNTs, which might have acted as a barrier disturbing the chain compactness [45] given sufficient time for crystallization. Because the annealing temperature is much higher than the glass transition of PLA, and annealing times are sufficient for crystallization, almost all the chain segments of PLA have sufficient mobility and time to crystallize without a nucleating agent. Therefore, the neat PLA (without MWCNTs to disturb full chain packing) showed higher crystallinity than did the PLA/MWCNT nanocomposites.

3.2. Thermal properties

The thermal behavior of the PLA/MWCNT nanocomposites has been investigated using DSC. As shown in Fig. 3(a), the endothermic melting peaks decreased to lower temperature in the presence of MWCNTs, suggesting an interaction between PLA and MWCNTs [56]. The decrease in the cold crystallization temperature of the PLA/MWCNT nanocomposites supported the nucleating effect of MWCNTs. Unusually, weak exothermic peaks were observed to the left of the endothermic melting peak of the PLA/MWCNT nanocomposites and were more prominent in the presence of MWCNTs. This phenomenon is the result of the transition of the α'-phase to the more stable α-phase during the DSC heating traces [43], supporting the interpretation that a disorder-to-order transition of the PLA crystal is effected by MWCNTs. The α'- and α-phases of PLA show distinct melting behaviors, as found in other studies [44,52,54]. After the annealing process at 120 °C, dual melting peaks were found, as shown in Fig. 3(b), because of two main mechanisms: the α'-to-α transition and melt recrystallization of the α-phase. The α'-to-α transition is generated and the complex system of the initial α'-phase and α-phase formed during the annealing process is generated. The existence of different crystal structures may result in the multiple melting peaks [44]. Theoretically, the α'-to-α transition is generally an exothermic process, while the melt recrystallization of the α-phase crystal formed in the annealing process is an endothermic process [43]. The second melting peak is more prominent in the PLA/MWCNT nanocomposites, while the first melting peak is more noticeable in the neat PLA. This result also supports the idea that an α'-to-α transition is induced by MWCNTs.

3.3. Interaction between PLA and MWCNTs

In previous studies [39], rheological analysis of PLA/MWCNT nanocomposites suggested a structural interconnection between PLA and MWCNTs because of their interaction. In order to quantify the

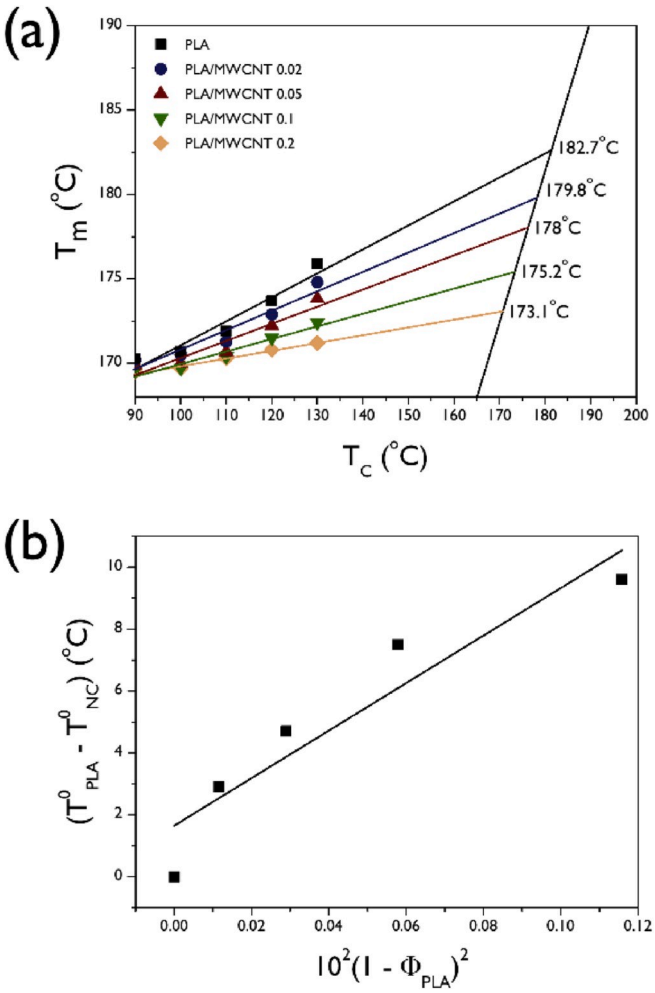

Fig. 4. (a) Hoffman-Weeks plot for the neat PLA and PLA/MWCNT nanocomposites and (b) Plot to obtain the interaction parameter in Nishi-Wang equation.

interaction between PLA and MWCNTs, the depression of the equilibrium melting point of PLA/MWCNT nanocomposites was investigated. The relationship between the Flory-Huggins interaction parameter (χ) and the equilibrium melting point depression can be analyzed using the following well-known Nishi-Wang equation [57,58]:

$$T^0_{PLA} - T^0_{NC} = -\frac{BV_u}{\Delta H_u} T^0_{PLA} (1 - \varphi_{PLA})^2$$

where T^0_{PLA} and T^0_{NC} are the equilibrium melting temperatures of the

Table 2
Thermal degradation parameters and activation energy of the PLA.

Materials	T_{id} (°C)	T_{dm} (°C)	W_R (%)	Horowitz-Metzger	
				E_a (kJ)	r^2
PLA	316.2	397.7	0.7	21.3	0.99
PLA/MWCNT 0.02	318.1	400.7	1.1	22.7	0.99
PLA/MWCNT 0.05	328.2	405.8	1.2	24.8	0.99
PLA/MWCNT 0.1	337.8	411	1.5	25.3	0.99
PLA/MWCNT 0.2	340.2	421.7	2.3	30.1	0.99

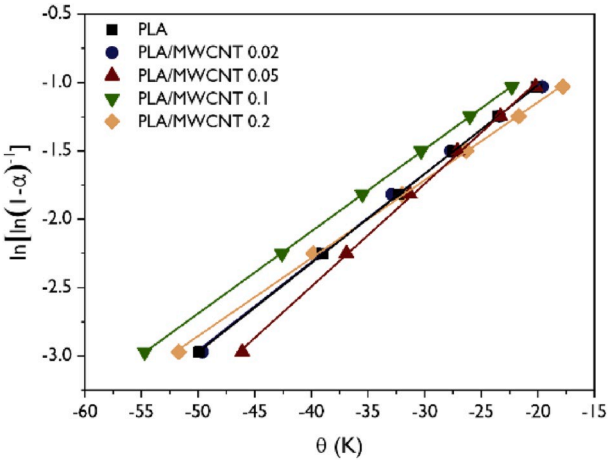

Fig. 5. Plots of Horowitz-Metzger method for PLA/MWCNT nanocomposites as a function of the θ.

neat PLA and nanocomposites, respectively. $\Delta H_u/V_u$ is the heat of fusion of PLA per unit volume and Φ_{PLA} is the volume fraction of PLA. B is the function of the interaction parameter (χ) and is defined as $\chi RT/V_u$. The R is the universal gas constant, and V_{PLA} is the molar volume of PLA. The ΔH_u and V_u values are calculated from the density of PLA (1.28 g/cm^3) and the melting enthalpy of 100% crystalline PLA (93.7 J/g) [59].

The equilibrium melting temperature is one of the most important parameters for the comprehension of crystallization and is defined as the melting temperature of infinite stacking crystals. The T^0_{PLA} and T^0_{NC} values were determined from the Hoffman-Weeks plots [60], which use the extrapolated intersections of the T_m vs T_c lines for various MWCNT contents with the $T_m = T_c$ line. The Hoffman-Weeks plots for the PLA/MWCNT nanocomposites are shown in Fig. 4(a): the equilibrium melting temperatures of PLA/MWCNT nanocomposites decreased with increasing MWCNT concentration, implying the less perfect crystallization of PLA in the presence of MWCNTs because of the hindrance effect of the nanotubes, which disturb the polymer chain packing.

The dependence of PLA content on the depression of the equilibrium melting temperature is shown in Fig. 4(b). The B value can be determined from the slope of the plot of $T^0_{PLA} - T^0_{NC}$ against $(1- \Phi_{PLA})^2$ and the obtained B value is -20.2 J/cm^3, implying that PLA and MWCNTs can form a thermodynamically compatible mixture above the melting temperature [58]. The moderate interaction between PLA and MWCNTs results from the dipolar interaction between the π cloud of MWCNTs and the carbonyl group of PLA [56].

3.4. Thermal stability

Thermal stability of polymer is an important property for applications because it determines the upper limit of service temperature. The MWCNTs was well known as a good physical barrier in the polymer matrix, retarding the thermal degradation of the polymer nanocomposites [61]. Initial degradation temperature (T_{id}), thermal degradation temperature at the maximum rate (T_{dm}), and residual yield (W_R), which were associated with enhancement of the thermal stability, are summarized in Table 2. The overall results for thermal stability indicated that the MWCNTs improved the thermal stability of PLA. For characterizing the effect of the MWCNT on the thermal stability of PLA, the following Horowitz-Metzger integral kinetic equation [62] was used to obtain the activation energy for thermal degradation (E_a).

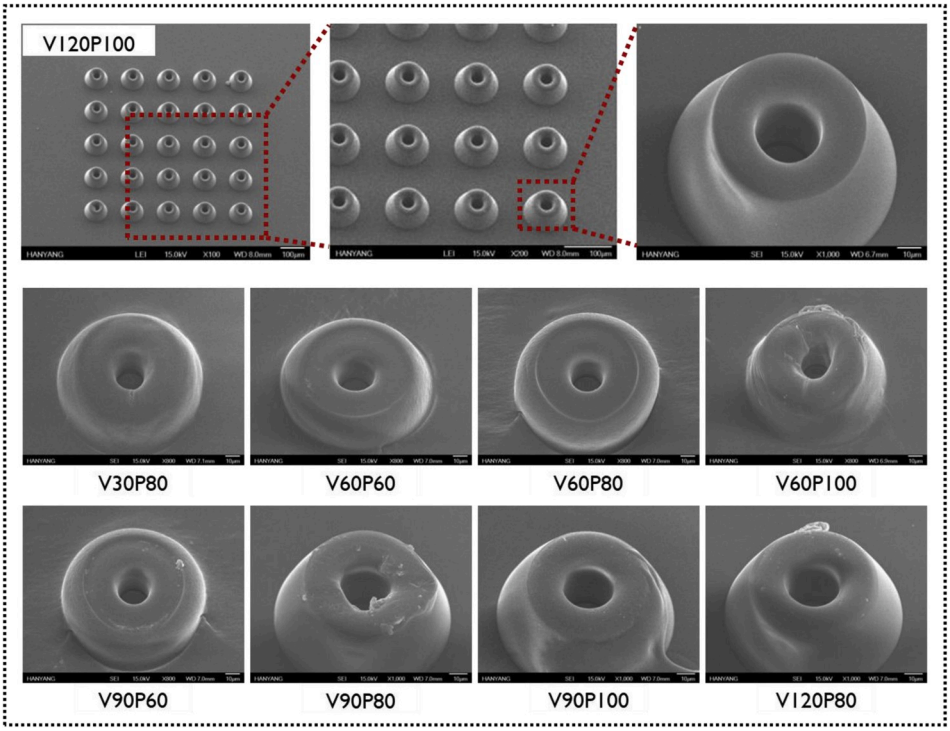

Fig. 6. SEM images of the micro needle surfaces of PLA at different injection speed (V) and holding pressure (P).

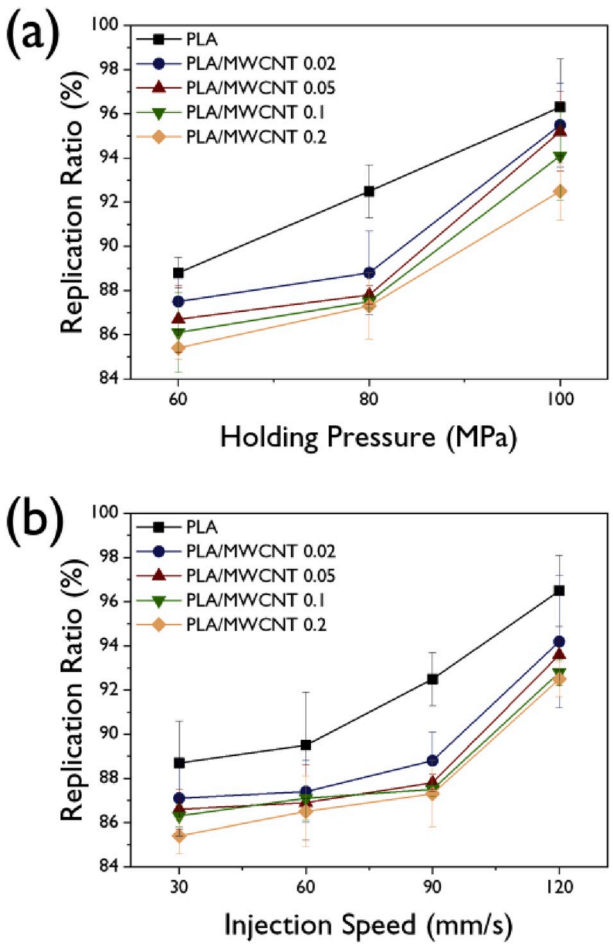

Fig. 7. Replication ratio of the neat PLA and PLA/MWCNT nanocomposites with (a) holding pressure at a constant injection speed of 90 mm/s and (b) injection speed at a constant holding pressure of 80 MPa.

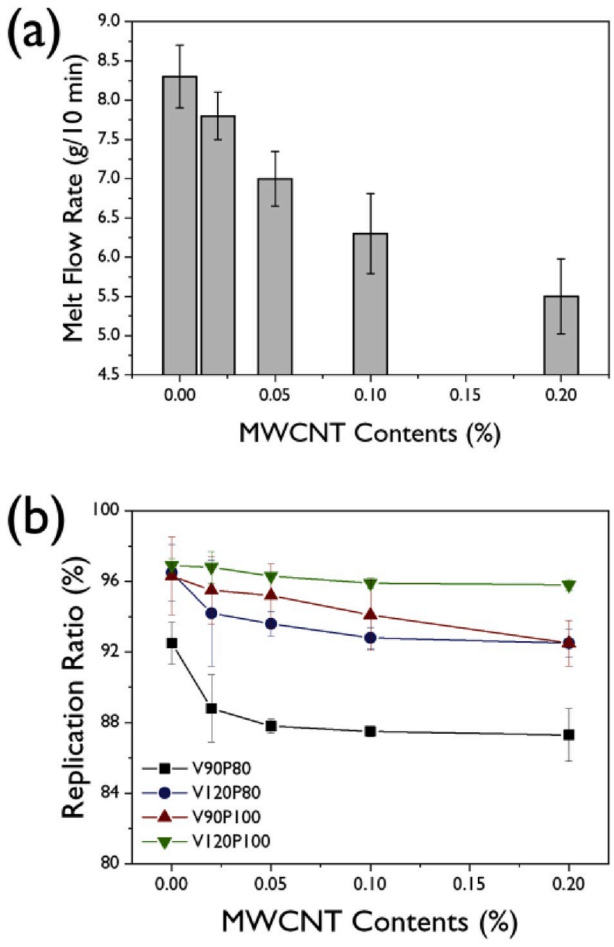

Fig. 8. (a) Melt flow index of PLA/MWCNT nanocomposites and (b) Replication ratio of the neat PLA and PLA/MWCNT nanocomposites at certain processing conditions with various MWCNT contents.

$$\ln\left[\boldsymbol{ln}(1-\boldsymbol{\alpha})^{-1}\right]=\frac{\boldsymbol{E_a\theta}}{\boldsymbol{RT_{dm}^2}}$$

where α and θ are the fractional weight loss and the difference between T and T_{dm}, respectively. The E_a can be calculated from the slop of the plots of $\ln[\ln(1-\alpha)^{-1}]$ against θ for all samples, as shown in Fig. 5. The obtained E_a values of PLA/MWCNT nanocomposites indicated that the physical barrier effect of the MWCNTs lead to higher E_a value, suggesting that the more energy was needed for thermal degrading of PLA/MWCNT nanocomposites.

3.5. Replication quality

Varying the injection speed and holding pressure resulted in different melt flows of the PLA/MWCNT nanocomposites in the mold during micro injection molding, leading to changes in the surface morphology of the microfeatures. The surface morphology of PLA/MWCNT nanocomposites is shown in Fig. 6. The micro needle patterns were well replicated at high holding pressures and injection speeds, while the microfeatures were not replicated at lower holding pressures and injection speeds. Smooth surfaces and clear edge definition in the microfeatures of PLA/MWCNT nanocomposites emerged at holding pressure of 120 MPa and injection speed of 100 mm/s. The effect of holding pressure and injection speed on the replication ratio of microfeatures are shown in Fig. 7 (a) and (b), respectively. Representative confocal images for the all PLA/MWCNT nanocomposites are shown in Fig. S1. The replication ratio increased with an increase in pressure and speed, implying that an increase of both the holding pressure and injection speed promoted complete filling of the mold with the polymer melt. However, the replication ratio of the microfeatures decreased in the presence of MWCNTs, which seem to have disturbed the PLA melt flow, as confirmed by the MFR analysis (Fig. 8 (a)). A rheological analysis of PLA/MWCNT nanocomposites was conducted previously [39], and the interaction between PLA and MWCNTs through their interconnected structure was found to increase the melt viscosity of PLA/MWCNTs nanocomposites. In micro injection process, viscosity is influenced more by shear rate, which is caused by injection speed, than melt or mold temperature. The shear-thinning effect can decrease the polymer melt viscosities, which enhances the material filling ability within the micro cavity. Moreover, the polymer can be shaped more completely after suffering sufficient holding pressure to prevent shrinkage. Although MWCNTs disturbed the melt flow of PLA/MWCNT nanocomposites by increasing melt viscosity, high holding pressures and injection speed increased the replication ratio of PLA/MWCNT nanocomposites. As shown in Fig. 8 (b), the micro injection molded PLA/MWCNT nanocomposites with replication ratio greater than 96%, were achieved at 100 MPa holding pressure and 120 mm/s injection speed.

3.6. Nanoindentation

Nanoindentation provides valuable quantitative information regarding the mechanical properties of various materials at the first surface layers [63]. This useful technique has been employed for polymeric systems, such as poly(ethylene oxide), poly(acrylic acid) [64],

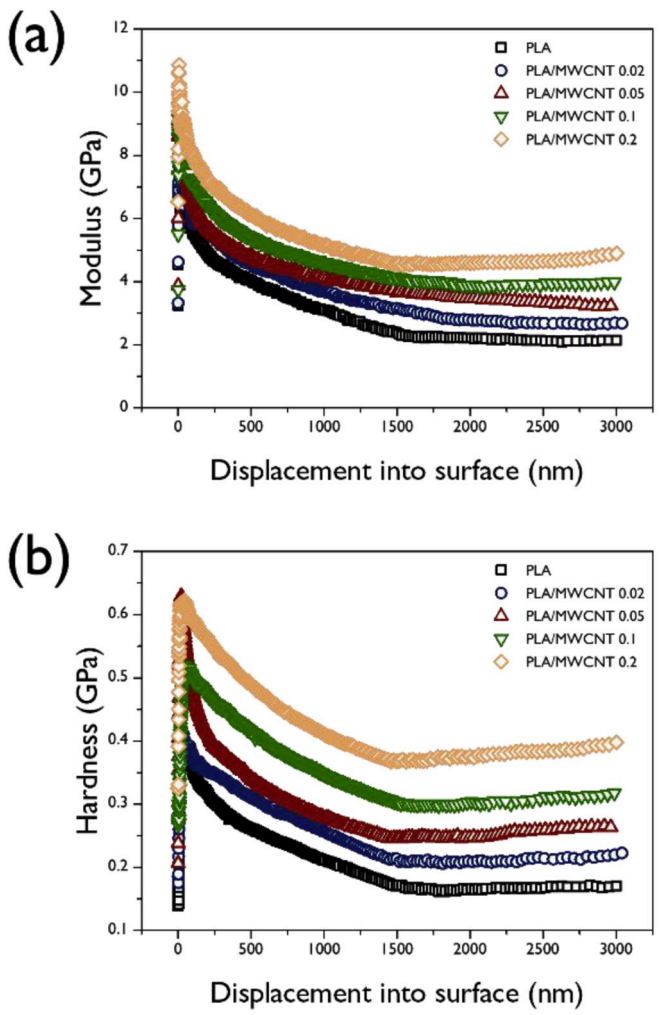

Fig. 9. Surface modulus (a) and hardness (b) of the neat PLA and PLA/MWCNT nanocomposites as a function of the displacement into surface.

poly(ethylene terephthalate) [65], and polyamide 6 and their composites [66]. A nanoindentation analysis was performed to probe the surface mechanical properties of PLA/MWCNT nanocomposites in this research, and the surface modulus and hardness with respect to the indentation depth are shown in Fig. 9 (a) and (b). Both the surface modulus and hardness were enhanced as a function of MWCNT concentration because of the addition of the stiff nanofiller into the matrix. Decrease in the surface modulus and hardness were also observed with increasing indentation depth because of the indentation size effect [67]. The surface modulus and hardness of PLA/MWCNT nanocomposites were roughly stabilized from 1500 nm onward. At 0.2 wt% MWCNTs, the surface modulus and hardness curves of the PLA were shifted upward slightly with increasing indentation depth. This upward shift might be the result of inhomogeneous MWCNT dispersion, because the neat PLA and PLA samples with lower MWCNT contents showed almost stable values of surface modulus and hardness [68]. From the results of our measurements, it appears that MWCNTs resulted in an improved hardness and surface modulus in the PLA, which are strongly related to the degree of crystallinity [69]. In many studies [35–37,39,70], the CNTs played a role as a nucleating agent in the PLA matrix and prompted heterogeneous nucleation. This nucleating effect of MWCNTs increased the crystallinity of PLA, leading to an improved surface modulus and hardness.

4. Conclusions

In this research, micro injection molded PLA/MWCNT nanocomposites with high surface quality were achieved by increasing the holding pressure and injection speed which promoted complete filling of the mold with the polymer melt. The surface mechanical properties of the PLA/MWCNT nanocomposites have been evaluated using a nanoindentation technique, and the surface modulus and hardness were improved by the stiff MWCNTs which led to crystallinity improvement though the α'-to-α-phase crystal transition of PLA. The MWCNT induced α′-to-α transition was confirmed by XRD and thermal analysis. The interaction between the PLA and MWCNTs was investigated using DSC to determine the depression of the equilibrium melting point of PLA/MWCNT nanocomposites. The estimated interaction parameter, *B*, was -20.2 J/cm^3 in the PLA/MWCNT system, indicating a thermodynamically compatible mixture. The activation energy for thermal degradation of the PLA/MWCNT nanocomposites reflected that the MWCNTs lead to improve thermal stability of PLA. This research has demonstrated the positive effect of MWCNTs on PLA for the development of micro injection molded polymers with excellent performance. The micro needle arrays can be applied as optical devices and miniaturized electrical devices.

Declaration of competing interest

The authors declare that they have no known competing financial interests or personal relationships that could have appeared to influence the work reported in this paper.

Acknowledgments

This research was supported by the Basic Science Research Program through the National Research Foundation of Korea (NRF) funded by the Ministry of Education (2016R1A6A1A03013422 and 2019R1F1A1062528).

Appendix A. Supplementary data

Supplementary data to this article can be found online at https://doi.org/10.1016/j.polymertesting.2019.106321.

References

[1] J. Giboz, T. Copponnex, P. Mélé, Microinjection molding of thermoplastic polymers: a review, J. Micromech. Microeng. 17 (2007) R96–R109.
[2] J. Giboz, T. Copponnex, P. Mélé, Microinjection molding of thermoplastic polymers: morphological comparison with conventional injection molding, J. Micromech. Microeng. 19 (2009).
[3] K. Park, S.-I. Lee, Localized mold heating with the aid of selective induction for injection molding of high aspect ratio micro-features, J. Micromech. Microeng. 20 (2010).
[4] H. Ito, H. Suzuki, K. Kazama, T. Kikutani, Polymer structure and properties in micro- and nanomolding process, Curr. Appl. Phys. 9 (2009) e19–e24.
[5] K.F. Zhang, Z. Lu, Analysis of morphology and performance of PP microstructures manufactured by micro injection molding, Microsyst. Technol. 14 (2007) 209–214.
[6] M. Fischer, P. Pöhlmann, I. Kühnert, Morphology and mechanical properties of micro injection molded polyoxymethylene tensile rods, Polym. Test. 80 (2019) 106078.
[7] Z. Liu, X. Liu, L. Li, G. Zheng, C. Liu, Q. Qin, L. Mi, Crystalline structure and remarkably enhanced tensile property of β-isotactic polypropylene via overflow microinjection molding, Polym. Test. 76 (2019) 448–454.
[8] Y.-C. Su, J. Shah, L. Lin, Implementation and analysis of polymeric microstructure replication by micro injection molding, J. Micromech. Microeng. 14 (2004) 415–422.
[9] L. Yu, C.G. Koh, L.J. Lee, K.W. Koelling, M.J. Madou, Experimental investigation and numerical simulation of injection molding with micro-features, Polym. Eng. Sci. 42 (2002) 871–888.
[10] F. Sammoura, J. Kang, Y.-M. Heo, T. Jung, L. Lin, Polymeric microneedle fabrication using a microinjection molding technique, Microsyst. Technol. 13 (2006) 517–522.
[11] D. Masato, M. Sorgato, G. Lucchetta, Analysis of the influence of part thickness on the replication of micro-structured surfaces by injection molding, Mater. Des. 95 (2016) 219–224.

[12] B. Sha, S. Dimov, C. Griffiths, M.S. Packianather, Investigation of micro-injection moulding: factors affecting the replication quality, J. Mater. Process. Technol. 183 (2007) 284–296.
[13] D. Yao, B. Kim, Scaling issues in miniaturization of injection molded parts, J. Manuf. Sci. Eng. 126 (2004) 733–739.
[14] R.E. Drumright, P.R. Gruber, D.E. Henton, Polylactic acid technology, Adv. Mater. 12 (2000) 1841–1846.
[15] R. Auras, B. Harte, S. Selke, An overview of polylactides as packaging materials, Macromol. Biosci. 4 (2004) 835–864.
[16] R.T. MacDonald, S.P. McCarthy, R.A. Gross, Enzymatic degradability of poly (lactide): effects of chain stereochemistry and material crystallinity, Macromolecules 29 (1996) 7356–7361.
[17] Y. Kikkawa, T. Suzuki, M. Kanesato, Y. Doi, H. Abe, Effect of phase structure on enzymatic degradation in poly (L-lactide)/atactic poly (3-hydroxybutyrate) blends with different miscibility, Biomacromolecules 10 (2009) 1013–1018.
[18] A.G. Mikos, M.D. Lyman, L.E. Freed, R. Langer, Wetting of poly (L-lactic acid) and poly (DL-lactic-co-glycolic acid) foams for tissue culture, Biomaterials 15 (1994) 55–58.
[19] Y. Ikada, H. Tsuji, Biodegradable polyesters for medical and ecological applications, Macromol. Rapid Commun. 21 (2000) 117–132.
[20] N. Kunou, Y. Ogura, M. Hashizoe, Y. Honda, S.-H. Hyon, Y. Ikada, Controlled intraocular delivery of ganciclovir with use of biodegradable scleral implant in rabbits, J. Control. Release 37 (1995) 143–150.
[21] X. Deng, J. Hao, C. Wang, Preparation and mechanical properties of nanocomposites of poly (D, L-lactide) with Ca-deficient hydroxyapatite nanocrystals, Biomaterials 22 (2001) 2867–2873.
[22] S. Saeidlou, M.A. Huneault, H. Li, C.B. Park, Poly(lactic acid) crystallization, Prog. Polym. Sci. 37 (2012) 1657–1677.
[23] T. Miyata, T. Masuko, Crystallization behaviour of poly (L-lactide), Polymer 39 (1998) 5515–5521.
[24] B. Na, N. Tian, R. Lv, Z. Li, W. Xu, Q. Fu, Evidence of sequential ordering during cold crystallization of poly (l-lactide), Polymer 51 (2010) 563–567.
[25] G.Z. Papageorgiou, D.S. Achilias, S. Nanaki, T. Beslikas, D. Bikiaris, PLA nanocomposites: effect of filler type on non-isothermal crystallization, Thermochim. Acta 511 (2010) 129–139.
[26] A.P. Mathew, K. Oksman, M. Sain, The effect of morphology and chemical characteristics of cellulose reinforcements on the crystallinity of polylactic acid, J. Appl. Polym. Sci. 101 (2006) 300–310.
[27] D. Wu, L. Wu, W. Zhou, M. Zhang, T. Yang, Crystallization and biodegradation of polylactide/carbon nanotube composites, Polym. Eng. Sci. 50 (2010) 1721–1733.
[28] H. Li, M.A. Huneault, Effect of nucleation and plasticization on the crystallization of poly(lactic acid), Polymer 48 (2007) 6855–6866.
[29] J.Y. Nam, S. Sinha Ray, M. Okamoto, Crystallization behavior and morphology of biodegradable polylactide/layered silicate nanocomposite, Macromolecules 36 (2003) 7126–7131.
[30] V. Krikorian, D.J. Pochan, Unusual crystallization behavior of organoclay reinforced poly (L-lactic acid) nanocomposites, Macromolecules 37 (2004) 6480–6491.
[31] V. Krikorian, D.J. Pochan, Crystallization behavior of poly (L-lactic acid) nanocomposites: nucleation and growth probed by infrared spectroscopy, Macromolecules 38 (2005) 6520–6527.
[32] E.J. Jeong, C.K. Park, S.H. Kim, Fabrication of microcellular polylactide/modified silica nanocomposite foams, J. Appl. Polym. Sci. (2019) 48616.
[33] H. Li, M. Huneault, Crystallization of PLA/thermoplastic starch blends, Int. Polym. Process. 23 (2008) 412–418.
[34] A. Pei, Q. Zhou, L.A. Berglund, Functionalized cellulose nanocrystals as biobased nucleation agents in poly(l-lactide) (PLLA) – crystallization and mechanical property effects, Compos. Sci. Technol. 70 (2010) 815–821.
[35] J.-Z. Xu, T. Chen, C.-L. Yang, Z.-M. Li, Y.-M. Mao, B.-Q. Zeng, B.S. Hsiao, Isothermal crystallization of poly(l-lactide) induced by graphene nanosheets and carbon nanotubes: a comparative study, Macromolecules 43 (2010) 5000–5008.
[36] X. Hu, H. An, Z.-M. Li, Y. Geng, L. Li, C. Yang, Origin of carbon nanotubes induced poly (L-lactide) crystallization: surface induced conformational order, Macromolecules 42 (2009) 3215–3218.
[37] Y. Zhao, Z. Qiu, W. Yang, Effect of functionalization of multiwalled nanotubes on the crystallization and hydrolytic degradation of biodegradable poly (L-lactide), J. Phys. Chem. B 112 (2008) 16461–16468.
[38] J.Y. Kim, H.S. Park, S.H. Kim, Unique nucleation of multi-walled carbon nanotube and poly(ethylene 2,6-naphthalate) nanocomposites during non-isothermal crystallization, Polymer 47 (2006) 1379–1389.
[39] S.H. Park, S.G. Lee, S.H. Kim, Isothermal crystallization behavior and mechanical properties of polylactide/carbon nanotube nanocomposites, Compos. Appl. Sci. Manuf. 46 (2013) 11–18.
[40] W. Hoogsteen, A. Postema, A. Pennings, G. Ten Brinke, P. Zugenmaier, Crystal structure, conformation and morphology of solution-spun poly (L-lactide) fibers, Macromolecules 23 (1990) 634–642.
[41] D. Brizzolara, H.-J. Cantow, K. Diederichs, E. Keller, A.J. Domb, Mechanism of the stereocomplex formation between enantiomeric poly (lactide) s, Macromolecules 29 (1996) 191–197.
[42] L. Cartier, T. Okihara, Y. Ikada, H. Tsuji, J. Puiggali, B. Lotz, Epitaxial crystallization and crystalline polymorphism of polylactides, Polymer 41 (2000) 8909–8919.
[43] P. Pan, B. Zhu, W. Kai, T. Dong, Y. Inoue, Polymorphic transition in disordered poly (L-lactide) crystals induced by annealing at elevated temperatures, Macromolecules 41 (2008) 4296–4304.
[44] P. Pan, W. Kai, B. Zhu, T. Dong, Y. Inoue, Polymorphous crystallization and multiple melting behavior of poly (L-lactide): molecular weight dependence, Macromolecules 40 (2007) 6898–6905.
[45] Y.-T. Shieh, G.-L. Liu, Y.-K. Twu, T.-L. Wang, C.-H. Yang, Effects of carbon nanotubes on dynamic mechanical property, thermal property, and crystal structure of poly(L-lactic acid), J. Polym. Sci. B Polym. Phys. 48 (2010) 145–152.
[46] G.Z. Voyiadjis, A. Samadi-Dooki, L. Malekmotiei, Nanoindentation of high performance semicrystalline polymers: a case study on PEEK, Polym. Test. 61 (2017) 57–64.
[47] D.D. Wright-Charlesworth, D.M. Miller, I. Miskioglu, J.A. King, Nanoindentation of injection molded PLA and self-reinforced composite PLA after in vitro conditioning for three months, J. Biomed. Mater. Res. Part A: An Official Journal of The Society for Biomaterials, The Japanese Society for Biomaterials, and The Australian Society for Biomaterials and the Korean Society for Biomaterials 74 (2005) 388–396.
[48] W.C. Oliver, J.B. Pethica, Method for Continuous Determination of the Elastic Stiffness of Contact between Two Bodies, Google Patents, 1989.
[49] A.C. Fischer-Cripps, E.F. Gloyna, W.H. Hart, Introduction to Contact Mechanics, Springer, 2000.
[50] B. Beake, S. Chen, J. Hull, F. Gao, Nanoindentation behavior of clay/poly (ethylene oxide) nanocomposites, J. Nanosci. Nanotechnol. 2 (2002) 73–79.
[51] J. Zhang, Y. Duan, H. Sato, H. Tsuji, I. Noda, S. Yan, Y. Ozaki, Crystal modifications and thermal behavior of poly (L-lactic acid) revealed by infrared spectroscopy, Macromolecules 38 (2005) 8012–8021.
[52] T. Kawai, N. Rahman, G. Matsuba, K. Nishida, T. Kanaya, M. Nakano, H. Okamoto, J. Kawada, A. Usuki, N. Honma, Crystallization and melting behavior of poly (L-lactic acid), Macromolecules 40 (2007) 9463–9469.
[53] M. Yasuniwa, K. Sakamo, Y. Ono, W. Kawahara, Melting behavior of poly(l-lactic acid): X-ray and DSC analyses of the melting process, Polymer 49 (2008) 1943–1951.
[54] J. Zhang, K. Tashiro, H. Tsuji, A.J. Domb, Disorder-to-order phase transition and multiple melting behavior of poly (L-lactide) investigated by simultaneous measurements of WAXD and DSC, Macromolecules 41 (2008) 1352–1357.
[55] J. Zhang, K. Tashiro, H. Tsuji, A.J. Domb, Investigation of phase transitional behavior of poly (L-lactide)/poly (D-lactide) blend used to prepare the highly-oriented stereocomplex, Macromolecules 40 (2007) 1049–1054.
[56] N.K. Singh, S.K. Singh, D. Dash, P. Gonugunta, M. Misra, P. Maiti, CNT induced β-phase in polylactide: unique crystallization, biodegradation, and biocompatibility, J. Phys. Chem. C 117 (2013) 10163–10174.
[57] T. Nishi, T. Wang, Melting point depression and kinetic effects of cooling on crystallization in poly (vinylidene fluoride)-poly (methyl methacrylate) mixtures, Macromolecules 8 (1975) 909–915.
[58] Z. Yu, J. Yin, S. Yan, Y. Xie, J. Ma, X. Chen, Biodegradable poly(l-lactide)/poly (ε-caprolactone)-modified montmorillonite nanocomposites: preparation and characterization, Polymer 48 (2007) 6439–6447.
[59] Z. Hong, P. Zhang, C. He, X. Qiu, A. Liu, L. Chen, X. Chen, X. Jing, Nano-composite of poly(L-lactide) and surface grafted hydroxyapatite: mechanical properties and biocompatibility, Biomaterials 26 (2005) 6296–6304.
[60] J.D. Hoffman, G.T. Davis, J. Lauritzen, Treatise on Solid State Chemistry, vol. 3, Plenum Press, New York, 1976, p. 497.
[61] S. Ho Park, S. Goo Lee, S.H. Kim, Thermal decomposition behavior of carbon nanotube reinforced thermotropic liquid crystalline polymers, J. Appl. Polym. Sci. 122 (2011) 2060–2070.
[62] H.H. Horowitz, G. Metzger, A new analysis of thermogravimetric traces, Anal. Chem. 35 (1963) 1464–1468.
[63] W.C. Oliver, G.M. Pharr, An improved technique for determining hardness and elastic modulus using load and displacement sensing indentation experiments, J. Mater. Res. 7 (2011) 1564–1583.
[64] M. Nowicki, A. Richter, B. Wolf, H. Kaczmarek, Nanoscale mechanical properties of polymers irradiated by UV, Polymer 44 (2003) 6599–6606.
[65] B. Beake, G. Leggett, Nanoindentation and nanoscratch testing of uniaxially and biaxially drawn poly (ethylene terephthalate) film, Polymer 43 (2002) 319–327.
[66] K. M, F. A, F.B. Calleja, F.S. x000E, Elastic properties of oriented polymers, blends and reinforced composites using the microindentation technique, Colloid Polym. Sci. 280 (2002) 591–598.
[67] W.D. Nix, H. Gao, Indentation size effects in crystalline materials: a law for strain gradient plasticity, J. Mech. Phys. Solids 46 (1998) 411–425.
[68] S.F. Wang, L. Shen, Y.J. Tong, L. Chen, I.Y. Phang, P.Q. Lim, T.X. Liu, Biopolymer chitosan/montmorillonite nanocomposites: preparation and characterization, Polym. Degrad. Stab. 90 (2005) 123–131.
[69] A. Peterlin, Drawing and extrusion of semi-crystalline polymers, Colloid Polym. Sci. 265 (1987) 357–382.
[70] Y.-Y. Liang, J.-Z. Xu, X.-Y. Liu, G.-J. Zhong, Z.-M. Li, Role of surface chemical groups on carbon nanotubes in nucleation for polymer crystallization: interfacial interaction and steric effect, Polymer 54 (2013) 6479–6488.